Hindawi
Advances in Materials Science and Engineering
Volume 2020, Article ID 4253026, 13 pages
https://doi.org/10.1155/2020/4253026

Research Article

Influence of Both Soil Properties and Geometric Parameters on Failure Mechanisms and Stability of Two-Layer Undrained Slopes

Shuangfeng Guo,[1,2] **Ning Li**,[1] **Wenpeng Liu**,[3] **Zongyuan Ma**,[1] **Naifei Liu**,[4] **and Gao Lv**[5]

[1]*State Key Laboratory of Eco-hydraulics in Northwest Arid Region, X'an University of Technology, Xi'an, Shaanxi 710048, China*
[2]*Department of Civil and Environmental Engineering, Colorado School of Mines, Golden, CO 80401, USA*
[3]*Earth Mechanical Institute, Department of Mining Engineering, Colorado School of Mines, Golden, CO 80401, USA*
[4]*School of Civil Engineering, Xi'an University of Architecture and Technology, Xi'an, Shaanxi 710055, China*
[5]*Mechanical Engineering College, Xi'an Shiyou University, Xi'an, Shaanxi 710065, China*

Correspondence should be addressed to Ning Li; ningli@xaut.edu.cn

Received 11 November 2019; Revised 4 May 2020; Accepted 18 May 2020; Published 27 June 2020

Academic Editor: Antonio Boccaccio

The stability of the two-layer undrained clay slopes should be given considerable attention since they are commonly observed in nature and in manmade structures, and they traditionally have low stability. Therefore, with the elastoplastic finite element method, this paper thoroughly explores the influence of the soil strength parameter c_u, slope angle β, and slope depth ratio DH on the slope stability and failure mechanisms by the wide-ranging parametric changes. The aims of this study are also to find the critical strength ratio $(c_{u2}/c_{u1})_{crit}$ and the maximum values of the stability number N_c that were observed in the parametric studies. Numerical results are displayed in the form of charts to give N_c and $(c_{u2}/c_{u1})_{crit}$ as a function of c_u, β, and DH. Moreover, influences of DH and β on N_c and failure mechanisms are examined in this study. The results of numerical analysis demonstrate that c_{u2}/c_{u1} significantly affects both the critical failure mechanism and the stability of the two-layer undrained slope. Improved knowledge of the location of the critical failure mechanism allows for accurately estimating the stability of the two-layer undrained slopes for future strengthening measurements to preserve stability.

1. Introduction

Slope stability analysis is a difficult and debatable problem and has been one of the most important areas of research in geotechnical engineering because it is probably one of the most complex and challenging issues in many geotechnical subdisciplines. Especially, the stability of the two-layer undrained slope has gained appreciable consideration in the research studies [1–7]. Investigators showed that two-layer undrained clay slopes are frequently encountered in the construction of embankments or dams and cutting slopes. In the past few decades, a lot of scholars assessed the slope stability, and they developed a quantity of advanced and effective methods over time for observing the behavior and failure mechanism of the slopes. Traditionally, limit equilibrium approaches assume a failure surface and require dividing the failing soil mass into slices (i.e., the ordinary method of slices [8], Bishop's methods [9], Morgenstern and Price's method [10], Spencer's method [11], and Janbu's generalized procedure of slices [12]). Most of these methods assume that the side force directions between slices as well as the shape of continuous failure surfaces need to be defined. The slope failure, from the local to the overall, is a progressive failure process in which the tensile stresses and the shear stresses are gradually released and transferred instead of the simultaneous destruction of all points in the slope. However, the failure criterion of the limit equilibrium method (*LEM*) is formulated according to the simultaneous failure of sliding surfaces but not the progressive failure process of the slopes.

Generally, the results indicate that traditional approaches simulate the slopes with highly homogeneous and

linear problems, but the actual slopes are usually anisotropic and heterogeneous. Moreover, traditional approaches fail to show discontinuous failure mechanisms which can result in conservative evaluation of the slope stability. Typically, the failure mechanisms of slopes have a remarkable increase in complexity, which is more likely to combine the deformation with the failure of the slopes. Therefore, just giving a conservative factor of safety (*FS*) to evaluate the yield and failure progress of the slopes does not capture the principal phenomena in slope stability analysis.

With the development of computer technology, slope stability analysis using the finite element method (*FEM*) has become a popular means and has been increasingly employed in geotechnical engineering practice during the past decades (e.g., [13, 14]). The advantages of using *FEM*, including enough accuracy and simplicity for slope stability analysis over conventional approaches, have been summarized by many specialists. As an alternative method to the *LEM*, the *FEM* with the strength reduction method (*SRM-FEM*) was suggested as early as in 1975 by Zienkiewicz et al [15]. and has been adopted in [15–17]. In addition to being one of the most powerful approaches for quantifying slope stability, *FEM* does not require that the shape and location of the potential sliding surface to be determined in advance, and the critical sliding surface could be naturally sought out when the soil shear strength is unable to maintain the applied shear stresses [18–22]. This method could be applied to receive information about the deformation, stress distribution, and the strain in the slope for different conditions such as rain and earthquake. Also, it can handle the complexity of geometries, boundary and loading conditions, varied soil properties, and the nonlinear stress-strain relationships [23]. In addition, *FEM* is able to single out the shear strength reduction of the landslide yield zone and monitor the progressive failure surface until the overall shear failure occurs.

The focus of this paper is to estimate the stability and to study the failure mechanism of two-layer undrained clay slopes consisting of different soil strengths. The transition point of the failure mechanism is introduced for one case by Griffiths and Lane [13]; based on this research, this paper considers the influence of different slope angles β and depth ratios D on the critical value of c_{u2}/c_{u1} and the corresponding critical failure mechanism of the slopes. *FEM* is then used to study c_{u2}/c_{u1}, β, and D on the stability number N_c. The paper thoroughly investigates the influences of the shear strength ratio c_{u2}/c_{u1}, the slope angle β, and the depth ratio D on slope stability and failure mechanisms of the slopes by wide-ranging parametric changes. Numerical simulations demonstrate that both the variances of geometry and soil properties of the slope can affect the stability and failure mechanisms of the two-layer undrained slopes.

2. Review of Methods and Mechanisms for Determining Slope Stability

2.1. Basic Assumptions. The program of the slope stability analysis involving the slope is subjected to gravity loads, and it has the ability to simulate slope situations with the variation of soil strength properties and geometric parameters. When this program is used to investigate the slope stability, several main assumptions are applied: (1) the nonlinear elastic-perfectly plastic constitutive model with the Mohr–Coulomb yield criteria assuming zero dilation is applied for two-dimensional plane strain analysis. (2) As a frictional material, the soil mass is ideal rigid and the soil model calls for four soil parameters: cohesion (c_u), Young's modulus (E), Poisson's ratio (υ), and the unit weight of the soil (γ). (3) The nonlinear problem is known as small-displacement analysis. The key target of this study follows the influence of the slope geometries and soil property variations on stability and the failure mechanisms of the slopes.

2.2. Strength Reduction Method (SRM). To implement slope stability analysis with the *FE* technique, the strength reduction factor (*SRF*) provides a quantitative indication of a slope, that is, for a series of the methodically reduced shear strength parameter c_{ur}, which is acquired by means of dividing the original strength parameters by a trial *SRF*. The reduced cohesion c_{ur} can be therefore defined as

$$c_{ur} = \frac{c_u}{SRF}, \tag{1}$$

where c_u is the original cohesion of the soil and c_{ur} is the reduced cohesion.

First of all, the gravity load program of the slope is simulated by the original strength parameter. Then, the *SRF* value incrementally increases until the slope failure just takes place. The critical value of *SRF* which is corresponding to slope failure can be regarded as the *FS* of the slope.

It is of great importance to determine the reasonably critical limit state, i.e., failure criteria and the critical failure mechanism of the slope. When determining the critical limit state, some common criteria used as indicators of slope failure are (1) a plastic yielding zone running through from the top to the toe of the slope. At failure, there is a plastic yielding band forming within the slope, and it would extend through the entire slope. However, the running through of the yielding zone is not an adequate situation for slope instability [24]. (2) Nonconvergence of the solution occurs [25]. Zienkiewicz et al. [15] proposed that a lack of convergence of the numerical solution is often taken as a symptom of slope failure. It is considered that nonconvergence would happen in the iteration of the system solution when the slope reaches the critical status. (3) A sharp increase in the maximum nodal displacements within the mesh appears. Griffiths and Lane [13] and Griffiths et al. [27] employed the dramatic increase in the nodal displacements within the mesh as an indicator of slope failure. In addition, most of the numerical examples demonstrate that this failure indicator has received more acceptance. When the stress distribution is unable to satisfy the failure indicator and the overall equilibrium at the same time, slope failure is considered to have occurred. Within the mesh, the

calculation program is required to supply an iteration ceiling beyond where the algorithm will stop attempting to redistribute the stresses. This paper utilizes indicator (3) that supplies an iteration ceiling of 2000 and introduces a ratio of the maximum nodal displacement $u_{\max}$ to the height of the slope H, i.e., maximum relative displacement $\delta_{\max} = u_{\max}/H$ (see Figure 1) is calculated in terms of SRF. Evidently, $\delta_{\max}$ is a monotonically increasing function.

2.3. Slope Stability Number in Strength Reduction. In a dimensionless manner, the theoretical number N_c is defined in view of the stability number put forward by Taylor [28]:

$$N_c = \frac{c_{u1}}{\gamma \cdot H \cdot FS}, \tag{2}$$

where FS is the factor of safety of the slope, γ is the unit weight of soil, and H is the slope height.

The failure surface of the slope is characterized by slope inclination angle β and depth ratio (DH), respectively, where DH is the depth from the slope crest to a firm stratum. Under the static loading condition, for $FS = 1$, the stability number N_c in equation (2) expresses the combination of c_u, γ, and DH, which warrants the slope to be at critical failure (limit equilibrium). When the slope's β and DH of the soil are given, then N_c can be calculated readily from Taylor's stability charts [29–33]. However, most of Taylor's original charts are for the homogeneous slopes, and these charts do not provide a common and easy means to assess the critical sliding surface related to a slope stability issue. Critical slip surfaces [34] determine the range of the potential failure region, and it is very important for evaluating slope analysis. This paper establishes not only the slope stability number N_c, but also the critical slip surface and failure mechanisms associated with stability numbers.

2.4. Failure Mechanisms of Slopes. For the purposes of determining the shape of a slope at failure and seeking out the most potential critical failure surface, this study considers slope failure mechanisms which can be divided into three different types: shallow failure mechanism, toe failure mechanism, and base deep failure mechanism [35–42]. Three failure mechanisms and their numerical characterizations are illustrated in Figure 2. It has been proven that the exact failure surface has a log-spiral shape, which has been widely utilized. In Figure 2, $Y_S(X)$ represents the slope surface and $Y_f(X)$ describes the critical slip surface. The origin of the coordinate system (X_C, Y_C) is located at the C point of the slope. The coordinates (X_O, Y_O) are the pole of the log-spiral with its circle points at the toe or the surface of the slope. (X_A, Y_A) or (X_B, Y_B) and (X_D, Y_D) are the coordinates where the failure surface intersects the slope surface which is associated with angle θ (the central angle defining the slip circle). Taylor [28] derived the relations of spiral radius R, X_O, and Y_O as follows.

For toe failure mechanism,

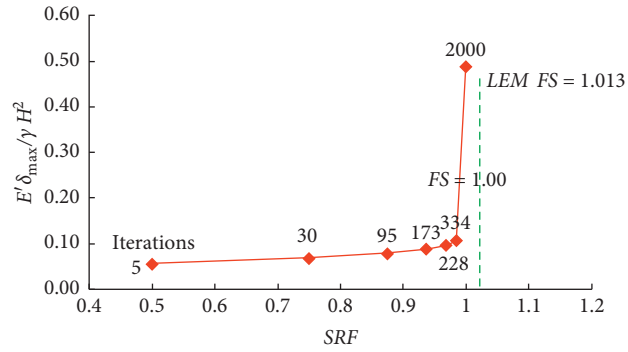

Figure 1: The rapid increase in the dimensionless displacement along with nonconvergence signifies slope failure, at which $FS = 1.00$ ($D = 1.5$, $c_{u2}/c_{u1} = 1.12$, and $\cot\beta = 1.0$).

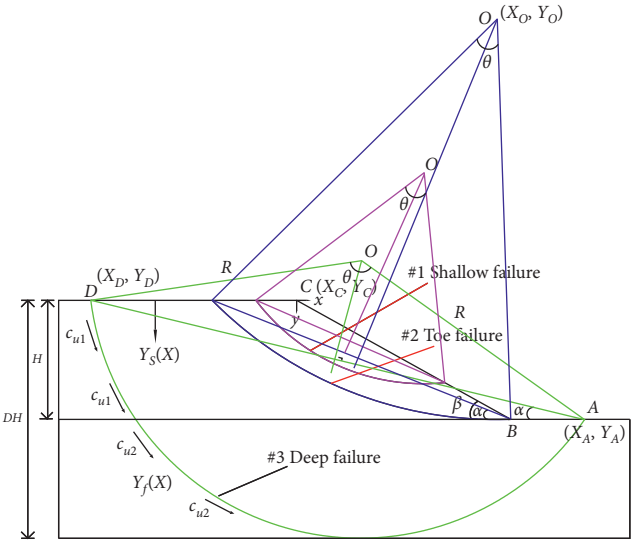

Figure 2: Three types of slope failure mechanisms of the finite slope.

$$R = \frac{H}{\sin\alpha \sin\theta};$$

$$Y_O = R\cos\left(\frac{\theta}{2} - \alpha\right); \tag{3}$$

$$X_O = R\sin\left(\frac{\theta}{2} - \alpha\right).$$

For base failure mechanism,

$$R = \frac{H}{\sin\alpha \sin\theta};$$

$$Y_O = R\cos\left(\frac{\theta}{2} - \alpha\right); \tag{4}$$

$$X_O = \frac{H}{2\tan\beta},$$

where α is the angle of the chord associating the start points and the end points (e.g., point D and point A) of the slip circle, θ is the central angle defining the slip circle, and β is the slope inclination angle.

Slope failures occur in three different failure mechanisms, depending on different parametric combinations of c_u, DH, and β. The shallow toe failure mechanism is shown as failure mechanisms #1 and #2 in Figure 2. The toe failure mechanism is where the failure surface passes through the toe of the slope (shown as #2 in Figure 2). The base deep failure mechanism indicates that the failure occurs with the failure surface passing at some distance below the toe of the slope (shown as failure mechanism #3 in Figure 2).

3. Numerical Modeling Setup

It is apparent that the effects of the variation of soil strength parameters are especially significant for the slopes on undrained clays. As indicated by the finite element analysis, the four parameters (c_u, E, υ, and γ) and appropriate boundary conditions should be considered due to their significant influences on the development of internal stresses of a slope. The stresses will influence the shape and location of the failure surface and the values of the minimum FS which correspond to the failure surface. The slope has the total unit weight $\gamma = 20\,\text{kN/m}^3$, the height $H = 18.0\,\text{m}$, and the undrained shear strength parameter $c_{u1} = 60.0\,\text{kPa}$, which are all held constant for calculating the FS or the stability number (N_c). The elastic parameters of Young's modulus (E) and Poisson's ratio (υ) are assigned to normal values of $10^5\,\text{kPa}$ and 0.3, respectively.

For the model demonstrated in this study, the slope is divided into two regions (embankment and foundation) to account for the slope properties. The undrained shear strength in the embankment is assigned as c_{u1} and thickness H, while the undrained shear strength of the foundation is appointed as c_{u2}. This paper considers using the ratio of c_{u2} to c_{u1} to represent the variation of strength parameters between the two distinct layers. The c_{u2}/c_{u1} ratio is named as P which varies from 0.2 to 3.5. Defining that $c_{u2}/c_{u1} < 1.0$ corresponds to the cases of a stiff clay-over-a soft clay layer, whereas $c_{u2}/c_{u1} > 1.0$ corresponds to the reverse. The slope geometry shown in Figure 3 has a foundation depth ratio DH, accounting for values ranging from 1.2 to 4.5, and the slope angle β ranges from 75° to 15° (namely, $\cot\beta = 0.286$–3.732). The boundary conditions for the parametric study are illustrated in Figure 3: horizontal displacements are fixed for nodes along the left and right boundaries and all displacements are fixed along the bottom boundary. Gravity loads are implemented to the mesh, and the trial factors of safety (SRF) gradually increase until nonconvergence occurs within the iteration ceiling in the mesh [43].

The critical value of P, herein named P_{crit}, represents the borderline value at which the critical mechanism changes from shallow to deep. For the two-layered clay system, P_{crit} is the function of combinations of $\cot\beta$ and D, which are utilized to analyze the failure mechanism of two-layer undrained slopes. The formulas of soil strength properties can be simply expressed in the following form:

$$P = \frac{c_{u2}}{c_{u1}},$$
$$P_{crit} = f(\cot\beta, D). \tag{5}$$

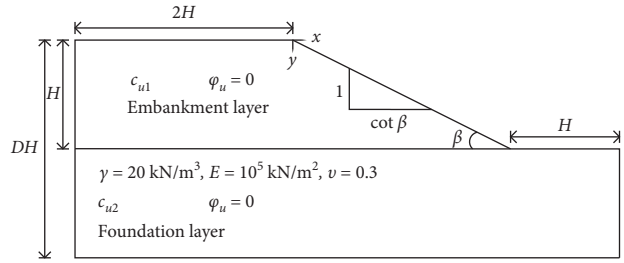

Figure 3: Two-dimensional geometry and input parameters for the slope model.

4. Numerical Modeling Results

4.1. Critical Strength Ratio c_{u2}/c_{u1}. The previous model determines the $\cot\beta$ and DH values, and it is also important to illustrate the critical value of c_{u2}/c_{u1} using an undrained slope example ($\varphi_u = 0$). It has a gradient of $\cot\beta = 1.5$ and $D = 1.5$. The geometry and finite element mesh of this slope are shown in Figure 4. The meshing utilized 8-node quadrilateral elements with reduced integration. Moreover, the model mesh has nels = 1800 elements and nn = 5635 nodes. In this slope, the undrained shear strength (c_{u2}) of the lower layer varies from 0.5 to 3.0, while other soil properties of embankment and foundation are kept constant, as mentioned above. Meanwhile, these slopes are calculated using FEM to make comparisons with the results obtained by LEM.

Table 1 lists the FS results and failure mechanisms of the slopes, both FEM and LEM. Figure 5 shows the curves of computed FS with a range of the c_{u2}/c_{u1} ratio. As expected, the results are very similar. A clear behavior change occurs at $c_{u2}/c_{u1} \approx 1.4$ with the finite element method, and an obvious discontinuity transition point is also at $c_{u2}/c_{u1} \approx 1.4$ with the LEM. That is, for this example, the critical c_{u2}/c_{u1} value is approximately 1.4. However, it may be noted that LEM requires the critical mechanism to be circular, while FEM places no restriction on its shape. Furthermore, the FS values are remarkably reduced when the foundation becomes weaker than the embankment. The foundation soil should be about 40% stronger than the embankment soil before the critical mechanism moves to the shallow location, at which the FS maintains a constant value after the critical c_{u2}/c_{u1}.

Figure 5 shows typical failure mechanisms corresponding to different values of c_{u2}/c_{u1}. It can be observed that the transition point at $P_{crit} = 1.4$ correlates with two failure mechanisms, indicating an ambiguous situation in which both shallow and deep mechanisms are trying to

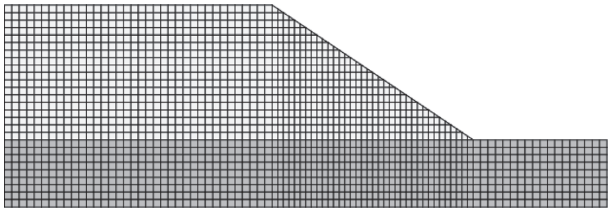

Figure 4: Typical mesh used for slope stability analysis.

Table 1: The computed *FS* and failure mechanisms of the slope for the case of $D = 1.5$ and $\cot\beta = 1.5$.

c_{u2}/c_{u1}	*FEM*		*LEM*	
	FS	Mechanisms	*FS*	Mechanisms
0.50	0.647	Deep	0.647	Deep
0.80	0.845	Deep	0.851	Deep
1.00	0.956	Deep	0.967	Deep
1.10	1.054	Deep	1.060	Deep
1.20	1.123	Deep	1.130	Deep
1.40	1.190	Two	1.185	Two
1.50	1.190	Shallow	1.185	Shallow
1.60	1.190	Shallow	1.185	Shallow
1.80	1.190	Shallow	1.185	Shallow
2.00	1.190	Shallow	1.185	Shallow
2.50	1.190	Shallow	1.185	Shallow
3.00	1.190	Shallow	1.185	Shallow

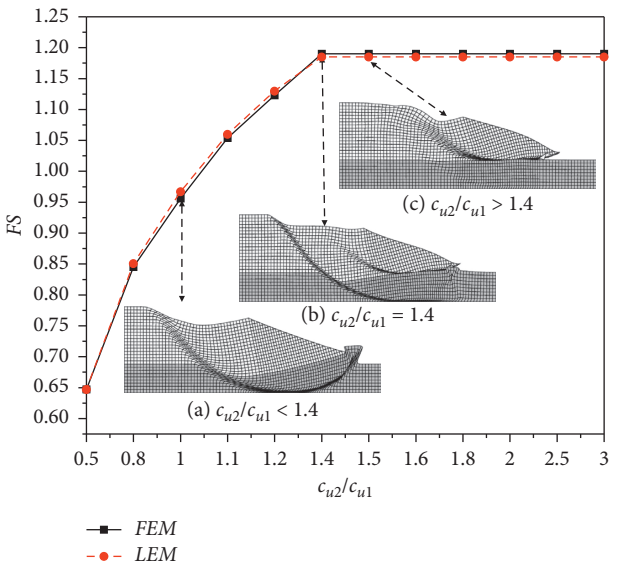

Figure 5: Computed *FS* and deformed meshes at failure for different strength ratio c_{u2}/c_{u1} ($D = 1.5$ and $\cot\beta = 1.5$).

form simultaneously. The corresponding critical failure mechanism should emphasize that both the values of $\cot\beta$ and D are the given values, and it is only c_{u2}/c_{u1} that is changing: $P < P_{crit}$ for deep failure mechanism (Figure 5(a)); $P = P_{crit}$ for two failure mechanisms of the slip surface (Figure 5(b)); $P > P_{crit}$ for shallow toe failure mechanism (Figure 5(c)). Furthermore, the results by

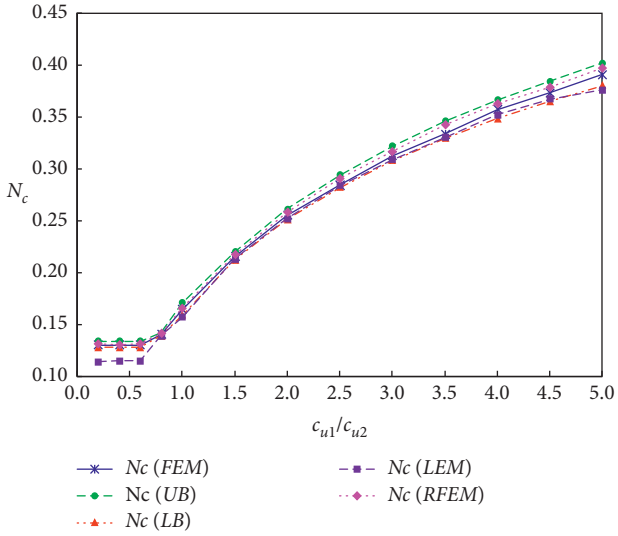

Figure 6: Comparison of N_c results by different methods.

FEM are compared with other results of four methods for each c_{u2}/c_{u1} ratio along the x axis. Figure 6 shows the stability number N_c results of the different methods.

It can be seen that the *FEM* results according to each c_{u2}/c_{u1} ratio plot between the results of the upper bound (*UB*) and the lower bound (*LB*) and are higher than the results of the *LEM* method. This phenomenon illustrates that *FEM* is very suitable to be used in practice directly to give a safe design. In general, there is no doubt that the failure mechanism relates to many influencing factors, not only the undrained strength property c_u but also the slope angle β and the depth ratio D. The study also investigates the influence of β and D on the failure mechanism and stability of different soil slopes.

Here, the paper defines "the two strongest surfaces" as the two most apparent failure mechanism circles, forming in the embankment and foundation soil layers at the same time. As the results show, the critical transition point P_{crit} is corresponding to the critical failure mechanism, which passes through two layers of the soil (two failure mechanisms). Therefore, the "two strongest failure mechanism" is the most interesting in that it involves two soil layers at the same time. The *FS* and failure mechanisms are estimated by *FEM* for the case slope compared with results obtained from *LEM*. The values of depth ratio $D = 1.5$ and a gradient $\cot\beta = 1.0$ are fixed, while c_{u2}/c_{u1} is varied in the range $c_{u2}/c_{u1} = 0.5, 0.8, \ldots, 3.0$. Figure 7 shows the results of *FEM* and *LEM*.

According to many trial computations, the results of the critical $c_{u2}/c_{u1} = 1.12$ (*FEM*) and the critical $c_{u2}/c_{u1} = 1.08$ (*LEM*) are obtained. When $SRF = 1.0$, there is a rapid increase in the dimensionless displacement $E\prime\delta_{\max}/\gamma H^2$, and the algorithm is unable to converge within the iteration limit 2000. Figure 1 shows the curve of dimensionless displacement against *SRF* for this case. The results of *LEM* are displayed in Figure 7(b), which obtains the minimum *FS* that corresponds to the critical c_{u2}/c_{u1} ratio and the critical failure surfaces of the slope. For these two failure surfaces, the

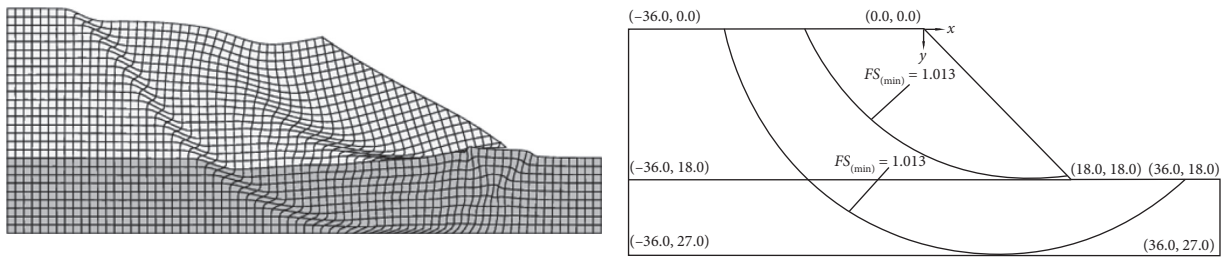

Figure 7: The "two strongest surface failure mechanism" for this case with two methods. (a) Deformed mesh at failure corresponding to the "two strongest surface mechanism" with *FEM*. (b) The "two strongest surface mechanism" with *LEM* and computed minimum factor of safety.

minimum *FS* is 1.013. As for the slope shown herein, the critical failure mechanism and the computed *FS* match well within the two methods.

4.2. Critical Failure Mechanisms. In order to investigate the influence of geometry of the slope (as shown in Figure 4) on slope stability and critical c_{u2}/c_{u1}, the stability numbers N_c, corresponding to different cotβ and c_{u2}/c_{u1}, can be easily obtained and are plotted in Figure 8 for the slope of $D = 1.5$. Referring to Figure 8, it can be observed that the stability number N_c decreases with c_{u2}/c_{u1} increasing at first and then maintains constant regardless of the change in the c_{u2}/c_{u1} ratios, just as expected. Taking into consideration equation (2) where N_c is proportional to the inverse of the *FS*, a higher N_c equates to a lower *FS* and vice versa. It can be found from Figure 8 that the arrow shows the direction of stability increasing. N_c decreases with increasing cotβ that is also expected. Based on equation (2) and Taylor's slope stability chart (Figure 2), it can be shown that N_c of the steep slope is higher than that of the flat slope when they have the same constant situation. In the case of steeper slopes, N_c could be as high as 0.54. The stability of a steeper slope is lower than that of a flatter slope in the same condition. Another phenomenon is that there are many definitely different transition points at the different ratios of c_{u2}/c_{u1}, and the *FS* of each transition point is the maximum value. The transition points also demonstrate that the different cotβ values correspond to the various critical failure mechanisms. The different transition points (P_{crit}) are obtained with various cotβ and constant $D = 1.5$ as shown in Table 2.

As shown in Figure 8 and Table 2, when cotβ increases, the critical c_{u2}/c_{u1} gradually increases. It should be noted that the maximum critical c_{u2}/c_{u1} is 1.6 for the case of cot$\beta = 3.732$ ($\beta = 15^\circ$), in which the strength of the lower soil is approximately 60% stronger than the upper soil. It means that the failure mechanism changes from the deep to the shallow toe when the ratio of c_{u2}/c_{u1} is just beyond the transition point 1.6. Concerning cot$\beta = 0.286$ ($\beta = 75^\circ$), it is noticed that the strength of the lower soil is equal to the upper soil ($c_{u2}/c_{u1} = 1.0$) before the deep failure mechanism becomes the most critical mechanism. This result indicates that cotβ makes a significant difference to the critical failure mechanism for slopes with the same D. Generally, most of the critical failure mechanisms corresponding to the transition points at P_{crit} are the two conflicting failure mechanisms. In addition, it should be known that the transitions of the failure mechanism are not only in terms of different cotβ, but also relate to different D. Therefore, the influence of cotβ and D on P_{crit} and the critical failure mechanisms has also been investigated at the same time in this paper. For many cases considered, Figure 9 presents the computed critical c_{u2}/c_{u1}, namely, P_{crit}, of purely cohesive two-layered ($\varphi_u = 0$) slopes. Further details and discussions are given below.

In Figure 9, on the whole, it can be clearly observed that when the D values are relatively high, such as $D = 1.8$ and $D = 2.0$, P_{crit} increases completely with the increase in the cotβ values. When D is large, the lower soil should be stronger than the upper soil before the critical mechanism moves to a shallow location. With the increasing of cotβ values, P_{crit} has many similar values when $D \leq 1.6$, especially for $D = 1.2$. Therefore, the slope angle, cotβ, has insignificant influence on the critical failure mechanism of the slopes for the very small D values. Increasing the D value leads to an increase in the cotβ influence on the critical failure mechanism. A positive correlation between P_{crit} and D is noticed, but it is just for some cases, such as the flatter inclination angle. For example, from cot$\beta = 2.0$ ($\beta = 26.57^\circ$) to cot$\beta = 3.732$ ($\beta = 15^\circ$), P_{crit} increases with the increase in the D values. Some of the results presented in Figure 9, however, illustrate that D cannot affect the values of P_{crit}, which keep constant no matter how the value of D changes for the relatively steeper slope cases. Further detailed observation reveals the P_{crit} has a large difference value between $D = 1.2$ ($P_{crit} = 1.4$) and $D = 2.0$ ($P_{crit} = 1.8$) when cot$\beta = 3.732$ ($\beta = 15^\circ$). This occurrence demonstrates that the changing of the critical failure mechanisms of flatter slopes is more strongly sensitive to various D values.

5. Stability and Failure Mechanism Analysis

5.1. Influence of Slope Geometry. Because the slope geometry has a great influence on the values of N_c, the variation of N_c for the different combinations of cotβ and D is shown in Figure 10. The values of c_{u2}/c_{u1} are equal to 0.5, 1.0, 1.5, and 3.0 from the stiff layer over the soft layer to the soft layer over

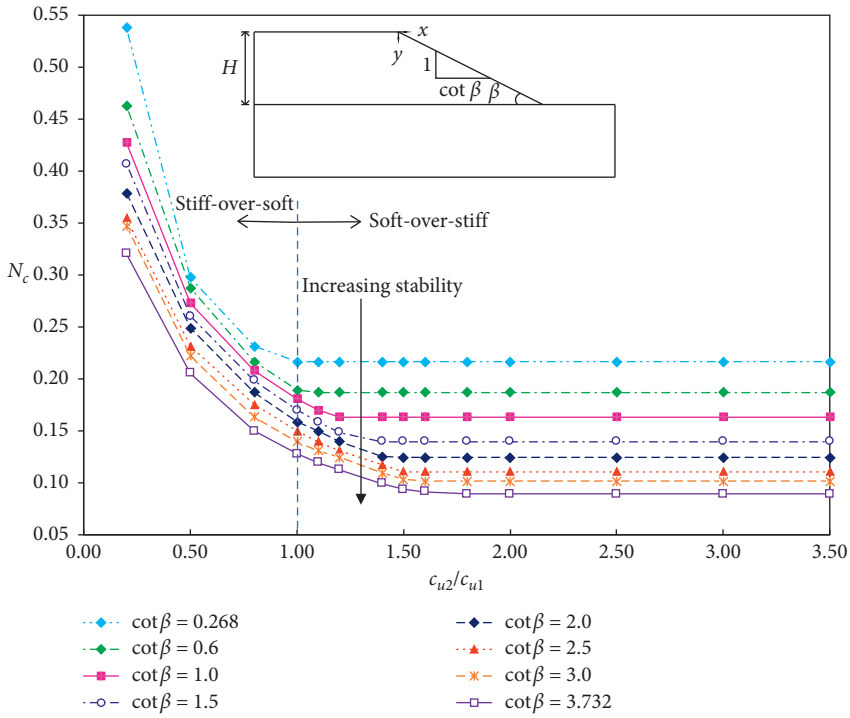

Figure 8: N_c and c_{u2}/c_{u1} for different values of cotβ ($D = 1.5$).

Table 2: P_{crit} corresponding to different cotβ and $D = 1.5$.

cotβ	$P_{crit} = (c_{u2}/c_{u1})_{crit}$
0.268	1.0
0.6	1.1
1.0	1.2
1.5	1.4
2.0	1.5
2.5	1.5
3.0	1.6
3.732	1.6

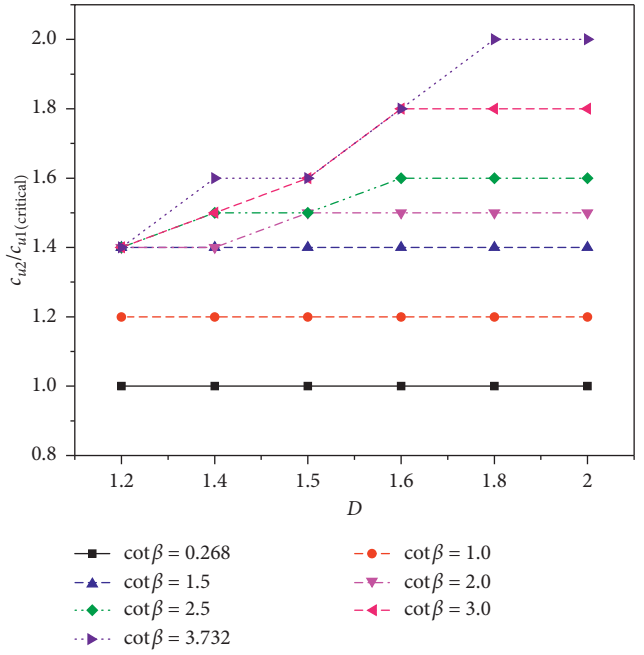

Figure 9: Computed P_{crit} corresponding to different cotβ and various D.

the stiff layer. For all values of c_{u2}/c_{u1}, by changing D values, in the range of (1.2, 1. 5. . ., 4.5), in all cases, the value of N_c decreases with increasing cotβ which makes a great influence on slope stability. For studying the influence of D on slope stability, similar curve plotting is carried out for the values of N_c, which are very close, or even coincide with each other for the soft layer-over-stiff layer slope. As illustrated in Figure 10(a), for $c_{u2}/c_{u1} = 0.5$ in the stiff layer over the soft layer, in all of cotβ, the values of N_c increase as the D values increase. That is, when the lower soil is weaker than the upper soil, the D values significantly influence slope stability. In general, the corresponding failure mechanism for $c_{u2}/c_{u1} = 0.5$ is a deep mechanism because of the weaker lower soil. *FEM* permits the failure mechanism of the slope to look for the weakest layer path through the soil mass, which can cause higher instability.

For the homogeneous undrained clay slope, $c_{u2}/c_{u1} = 1.0$, β is greater than 53°, the failure takes place along a circular slip surface passing through the toe, and this kind of circle arc is called a toe sliding surface. From Taylor's charts, for β greater than 53°, the failure circle may be always a toe circle. When β is less than 53°, the failure circle becomes toe, deep, and base circles (tangent to a firm base), depending on the values of D. Therefore, when $\beta > 53°$, the critical failure mechanism is consistently a toe circle, as shown in Figure 10(b). The value of D has no influence on the slope stability and failure mechanism if cot$\beta < 0.6$.

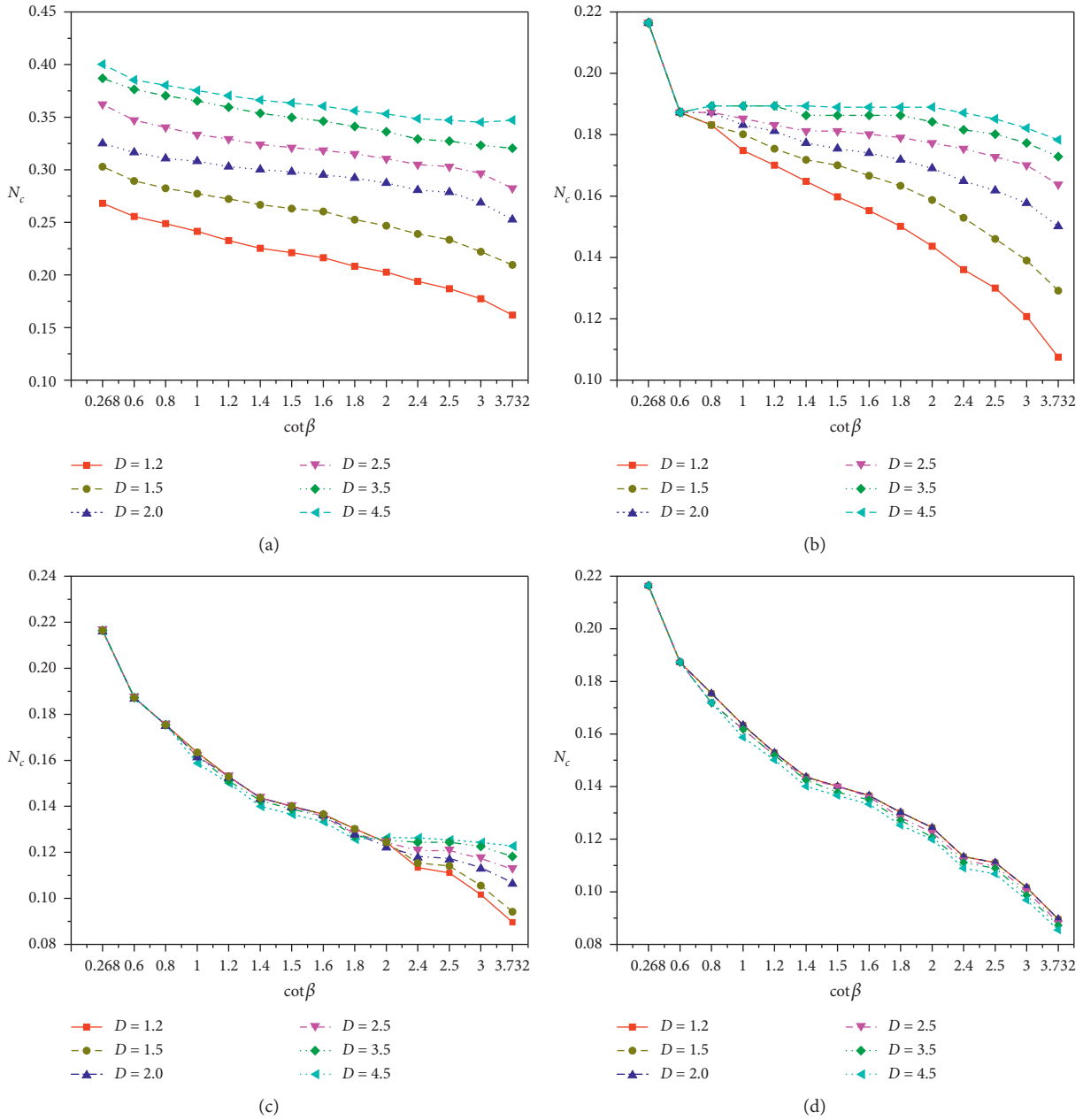

Figure 10: Continued.

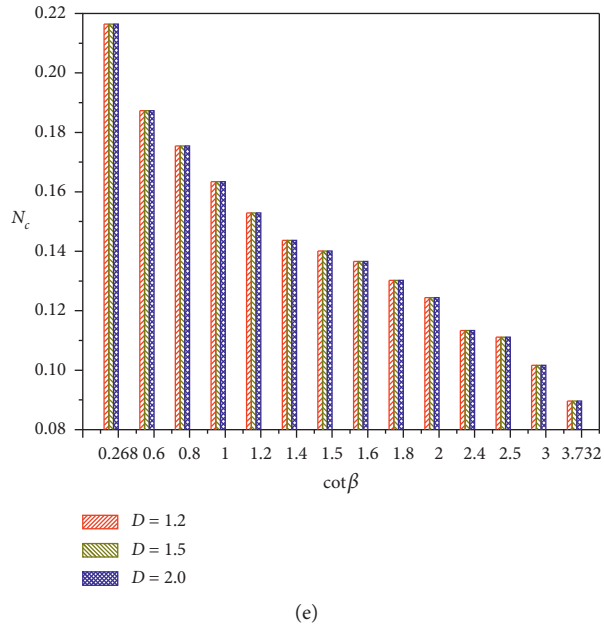

Figure 10: Influence of different cotβ and D on N_c of the undrained slope with various c_{u2}/c_{u1}. (a) $c_{u2}/c_{u1} = 0.5$ (stiff-over-soft). (b) $c_{u2}/c_{u1} = 1.0$ (uniform soil). (c) $c_{u2}/c_{u1} = 1.5$ (soft-over-stiff). (d) $c_{u2}/c_{u1} = 3.0$ (soft-over-stiff). (e) $c_{u2}/c_{u1} = 3.0$ (soft-over-stiff).

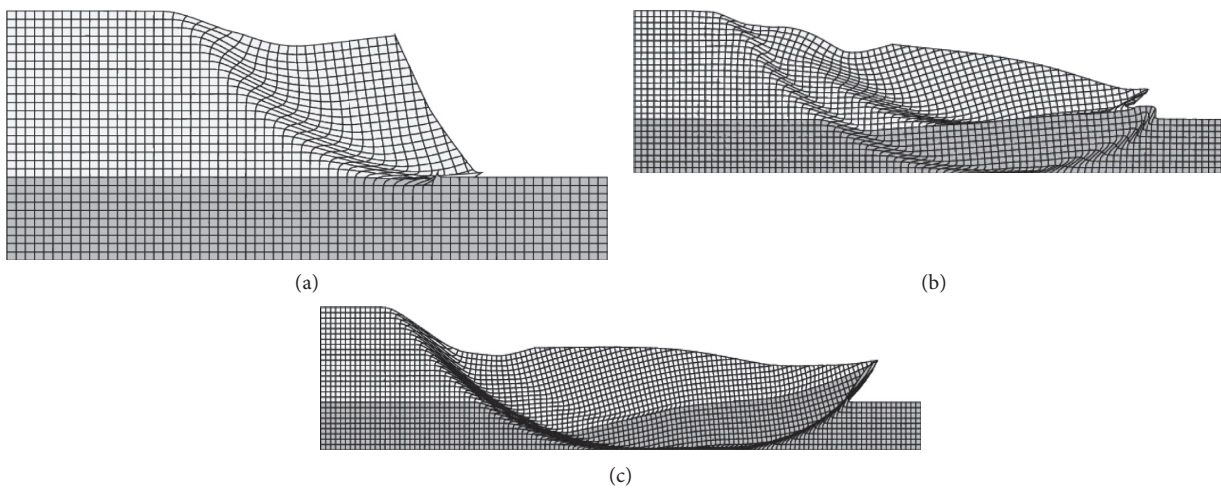

Figure 11: Deformed meshes at failure for different cotβ ($cu_2/cu_1 = 1.5$ $D = 1.5$). (a) cot$\beta = 0.268$ ($\beta = 75^\circ$). (b) cot$\beta = 2.2$ ($\beta = 24.44^\circ$). (c) cot$\beta = 3.732$ ($\beta = 15^\circ$).

As mentioned above, the slope angle β has a remarkable influence on slope stability and the failure mechanism as shown in Figure 10(c). It can be supported by the failure mechanisms illustrated in Figure 11. The *FE* deformed meshes indicates that, depending on the slope angle β, the failure mechanisms change from shallow to deep. It is interesting to highlight a toe mechanism at the steep slope of $\beta = 75^\circ$, as shown in Figure 11(a). The failure mechanism appears in two conflicting and ambiguous mechanisms at $\beta = 24.44^\circ$ as presented in Figure 11(b), and the deep mechanism is critical for the relatively flat slope at $\beta = 15^\circ$ as shown in Figure 11(c). For flatter undrained slopes, the typical failure mechanisms, as reported by Griffiths et al. [2], are that the failure mechanisms are nearly always deep and pass through the foundation soils. For steeper slopes, the failure mechanism has more potential actions and may go through the toe, leading to a higher N_c.

In addition, there is no notable shape variations in the failure mechanism for different D values in Figures 10(c)–10(d)), which indicates that N_c is almost independent of the slope depth D. Particularly, $D = 1.2$, 1.5, and 2.0, and all of the values of N_c are exactly the same for given cotβ, which is shown in the illustration in Figure 10(e). The reason for this phenomenon is that the slope stability is controlled by the

weaker soil, while lower layer soil strength is assumed to be three times stronger than that of the upper layer soil ($c_{u2}/c_{u1} = 3.0$). Thus, the lower layer soil should be considered as a rigid layer, and the upper layer soil plays a significant role in slope stability and failure mechanisms. The exactly equal values do not exist in the relatively large D values ($D = 2.5$–4.5), as shown in Figure 10(d), but the values of N_c are very close. All in all, the influence of D is less sensitive to slope stability and failure mechanism for the soft-over-stiff slopes.

Charts in Figure 10 indicate that the stability number N_c decreases with the increasing cotβ. All results received by the previously mentioned implementations illustrate that decreasing the slope angle β leads to an increased slope stability, irrespective of the variance of the strength parameters. For the stiff-over-soft slope system, the values of N_c are lower for slopes with a low slope depth ratio D than for slopes with a high slope depth ratio D. For the soft-over-stiff, the values of N_c are higher for slopes with a low slope depth ratio D than for slopes with a high slope depth ratio D. Further examination of those phenomena provided by the slopes shows that the failure mechanisms change from the shallow toe to two obvious failures and then to deep, which has relevance to β and D.

5.2. Influence of Slope Strength Parameter c_{u2}/c_{u1}. The accuracy of Figure 12 is confirmed for steep and flat slopes using the different values of c_{u2}/c_{u1} and D. It can be obviously observed that N_c increases with increasing D but decreases with increase in the ratio of c_{u2}/c_{u1}, when $c_{u2}/c_{u1} \le 1.0$ (stiff-over-soft). The value of N_c for the thick lower layer (e.g., $D > 1.8$) has clearly influenced various D values on the flat slope, where N_c has a obviously decreased tendency with increasing c_{u2}/c_{u1} for higher slopes. The influence of D on N_c is found to be less sensitive for the ratio of $c_{u2}/c_{u1} \ge 1.5$ (soft-over-stiff) for both flat and steep slopes. It is also noted that the steep slope ($\beta = 75^\circ$) has the same N_c values after $c_{u2}/c_{u1} = 1.0$, which implies that the FS is a constant value, regardless of the increasing D values. Therefore, D has almost no influence on the soft-over-stiff steep slope stability.

So, as to clearly understand the influence of D on the failure mechanism of the slopes, for cot$\beta = 2.0$ and $c_{u2}/c_{u1} = 1.5$ slopes, a series of computations and comparisons have been performed to obtain the results. Figure 13 displays the failure mechanisms with various D values. An interesting phenomenon is found that the depth of the failure surface increases with increasing D. It can be remarked that the failure mechanism stays shallow if there is a relatively thin foundation depth of $D = 1.5$ (Figure 13(a)); the failure mechanism involves both the shallow and deep failure mechanisms within two soils in the embankment and the foundation for $D = 1.8$ (Figure 13(b)), and a deep mechanism is preferred at $D = 2.0$ (Figure 13(c)). Hence, further exhaustive observation illustrates that the shallow-to-deep failure mechanisms are affected by increasing D values while holding c_{u2}/c_{u1} and cotβ values constant.

The strength ratio c_{u2}/c_{u1} has a greater influence on N_c for flat slopes than steep slopes. In addition, except for $c_{u2}/c_{u1} = 0.2$, 0.5, and 0.8, other c_{u2}/c_{u1} values cause the same N_c value for all D values in the steep slope. The influence of D on the failure mechanism for holding c_{u2}/c_{u1} and cotβ slope constant is that the increasing D corresponds to the shallow toe-to-deep mechanisms. For a lower slope, the failure mechanism has more choices and may go through the shallow and pass through the toe foundation soils. For a higher undrained slope, at least one failure surface is deep

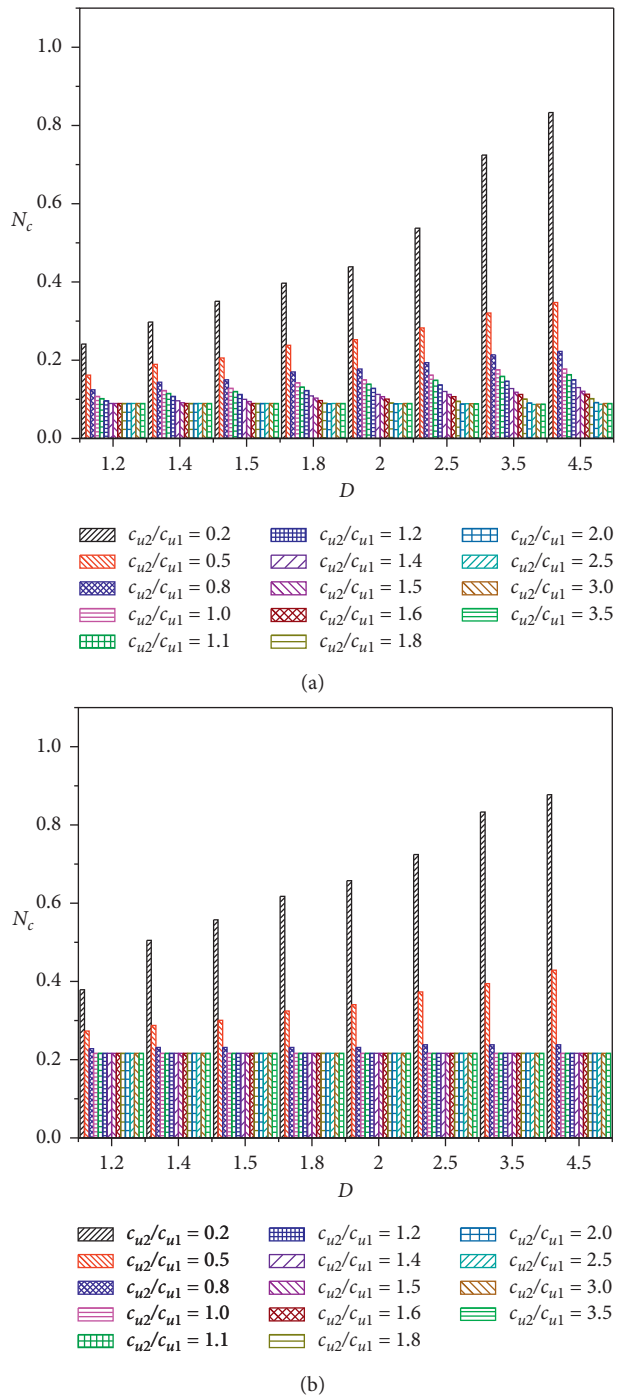

Figure 12: Influence of different D and c_{u2}/c_{u1} of undrained slope with various cotβ. (a) cot$\beta = 3.732$ ($\beta = 15^\circ$). (b) cot$\beta = 0.268$ ($\beta = 75^\circ$).

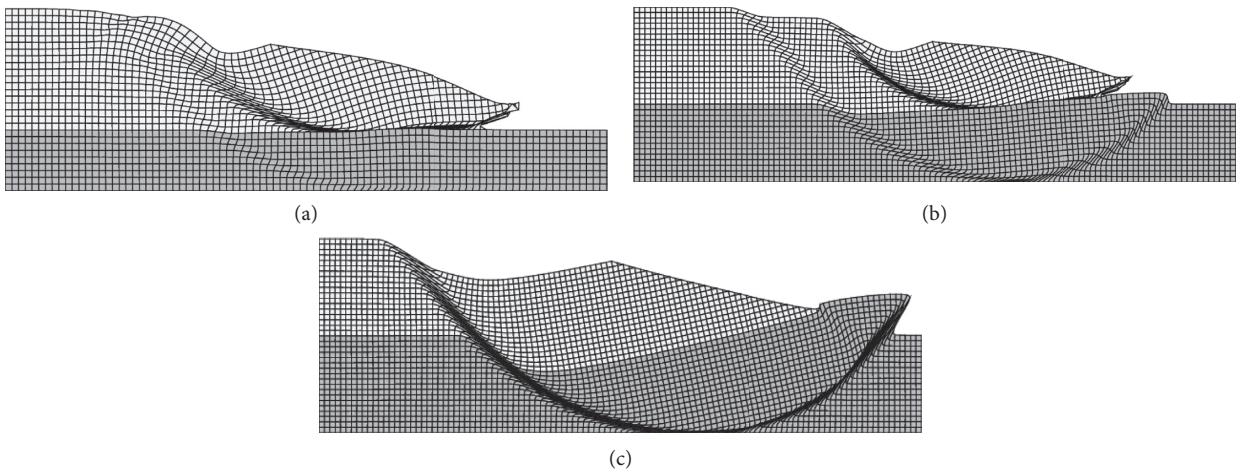

Figure 13: Deformed meshes at failure for different D values ($c_{u2}/c_{u1} = 1.5$, $\cot\beta = 2.0$). (a) $D = 1.5$. (b) $D = 1.8$. (c) $D = 2.0$.

and passes through the foundation soil, leading to higher slope instability probability.

6. Concluding Remarks

This paper has investigated the stability and the failure mechanism specifically of two-layer undrained clay slopes with varied soil shear strengths. The weaker soil always dominates the overall performance and results in slope instability. In addition, the failure mechanism seeks out the path of the weakest resistance through the soil mass. The critical strength ratio c_{u2}/c_{u1} and the distinct transition points of failure mechanisms of the two-layer slopes are obtained utilizing finite element analysis. More specific conclusions can be summarized from this study as follows [44]:

(1) The critical failure mechanism corresponding to the critical strength ratio $(c_{u2}/c_{u1})_{crit}$ involves a situation in which both shallow and deep mechanisms attempt to form simultaneously. For the flatter slopes, the critical c_{u2}/c_{u1} increases with the increase in slope depth D, but it has a negative relationship with the slope angle β. However, for the steeper slopes, $(c_{u2}/c_{u1})_{crit}$ does not depend on D, and it still increases as β decreases.

(2) Soil strength ratio c_{u2}/c_{u1} has notable effects on the stability of the two-layer undrained clay slope. For a stiff-over-soft clay slope ($c_{u2}/c_{u1} < 1.0$), the variation of the strength parameters has significant influences on the slope stability, so that the values of N_c are decreasing with increasing c_{u2}/c_{u1}. This effect is more remarkable with greater values of D. However, for a soft-over-stiff clay slope ($c_{u2}/c_{u1} > 1.0$), the variation of the strength parameters have slight influences on the slope stability.

(3) The slope stability is decreasing as the value of β increases. This situation is more noteworthy at higher values of strength ratio c_{u2}/c_{u1}. And, for another aspect, the variation of the strength parameters has more remarkable influences on the slope stability for flat slopes than that of steep slopes. The higher the values of D, the more obvious the influences of c_{u2}/c_{u1} on the stability of an undrained clay slope which can be observed in the flat slopes' context.

(4) This paper has performed stability charts to demonstrate the magnitude of N_c for different parametric (c_{u2}/c_{u1}, β, and D) combinations. Slopes with higher D result in lower stabilities than slopes with lower D for stiff-over-soft clay. Nevertheless, for soft-over-stiff slopes, it is noted that N_c is completely insensitive to the value of D, which is found to have few influences on slope stability.

(5) The failure mechanism of the slope will be changing gradually from the shallow toe to two failure surfaces and then to deep with the increase in both c_{u2}/c_{u1} and D and a decrease in β.

Data Availability

The data used to support the findings of this study are available from the corresponding author upon request.

Conflicts of Interest

The authors declare that there are no conflicts of interest regarding the publication of this paper.

Acknowledgments

The first author of the paper is grateful to the Chinese Scholarship Council (CSC) for providing a scholarship to conduct the research described in this paper at the Colorado School of Mines, Golden, CO, USA (CSC no. 201708610108). This study was supported by the Shaanxi Natural Science Foundation (Grant no. 2019JQ-756) and the Shaanxi Province Science Foundation for Youths (Grant no. 2018JQ5203).

References

[1] A. J. Li, R. S. Merifield, and A. V. Lyamin, "Limit analysis solutions for three dimensional undrained slopes," *Computers and Geotechnics*, vol. 36, no. 8, pp. 1330–1351, 2009.

[2] D. V. Griffiths, J. Huang, and G. A. Fenton, "Influence of spatial variability on slope reliability using 2-D random fields," *Journal of Geotechnical and Geoenvironmental Engineering*, vol. 135, no. 10, pp. 1367–1378, 2009.

[3] A. J. Li, R. S. Merifield, and A. V. Lyamin, "Three-dimensional stability charts for slopes based on limit analysis methods," *Canadian Geotechnical Journal*, vol. 47, no. 12, pp. 1316–1334, 2010.

[4] Z. G. Qian, A. J. Li, R. S. Merifield, and A. V. Lyamin, "Slope stability charts for two-layered purely cohesive soils based on finite element limit analysis methods," *International Journal of Geomechanics*, vol. 15, no. 3, Article ID 06014022, 2015.

[5] K. Lim, A. J. Li, and A. V. Lyamin, "Three-dimensional slope stability assessment of two-layered undrained clay," *Computers and Geotechnics*, vol. 70, pp. 1–17, 2015.

[6] J. K. Lee, S. Jeong, and J. Q. Shang, "Undrained bearing capacity of ring foundations on two-layered clays," *Ocean Engineering*, vol. 119, pp. 47–57, 2016.

[7] X.-Y. Li, L.-M. Zhang, L. Gao, and H. Zhu, "Simplified slope reliability analysis considering spatial soil variability," *Engineering Geology*, vol. 216, pp. 90–97, 2017.

[8] W. Fellenius, "Calculation of the stability of earth dams, transactions of the 2nd congress on large dams," *International Commission on Large Dams of the World Power Conference*, vol. 4, pp. 445–462, 1936.

[9] A. W. Bishop, "The use of the slip circle in the stability analysis of slopes," *Géotechnique*, vol. 5, no. 1, pp. 7–17, 1955.

[10] N. R. Morgenstern and V. E. Price, "The analysis of the stability of general slip surfaces," *Géotechnique*, vol. 15, no. 1, pp. 79–93, 1965.

[11] E. Spencer, "A method of analysis of the stability of embankments assuming parallel inter-slice forces," *Géotechnique*, vol. 17, no. 1, pp. 11–26, 1967.

[12] N. Janbu, "Slope stability computations," *Soil Mechanics and Foundation Engineering Report*, Technical University of Norway, Trondheim, Norway, 1968.

[13] D. V. Griffiths and P. A. Lane, "Slope stability analysis by finite elements," *Géotechnique*, vol. 49, no. 3, pp. 387–403, 1999.

[14] J. Chen, J.-H. Yin, and C. F. Lee, "Upper bound limit analysis of slope stability using rigid finite elements and nonlinear programming," *Canadian Geotechnical Journal*, vol. 40, no. 4, pp. 742–752, 2003.

[15] O. C. Zienkiewicz, C. Humpheson, and R. W. Lewis, "Associated and non-associated visco-plasticity and plasticity in soil mechanics," *Géotechnique*, vol. 25, no. 4, pp. 671–689, 1975.

[16] T.-K. Nian, R.-Q. Huang, S.-S. Wan, and G.-Q. Chen, "Three-dimensional strength-reduction finite element analysis of slopes: geometric effects," *Canadian Geotechnical Journal*, vol. 49, no. 5, pp. 574–588, 2012.

[17] H. W. Fang, Y. F. Chen, and Y. X. Xu, "New instability criterion for stability analysis of homogeneous slopes," *International Journal of Geomechanics*, vol. 20, no. 5, Article ID 04020034, 2020.

[18] D. V. Griffiths and G. A. Fenton, "Probabilistic slope stability analysis by finite elements," *Journal of Geotechnical and Geoenvironmental Engineering*, vol. 130, no. 5, pp. 507–518, 2004.

[19] J. Huang, D. V. Griffiths, and G. A. Fenton, "System reliability of slopes by RFEM," *Soils and Foundations*, vol. 50, no. 3, pp. 343–353, 2010.

[20] D. V. Griffiths, D. Zhu, J. Huang, and G. A. Fenton, "Observations on probabilistic slope stability analysis," in *Proceedings of the 6th Asian-Pacific Symposium on Structural Reliability and its Applications*, Shanghai, China, May 2016.

[21] S. Xiao, W. D. Guo, and J. X. Zeng, "Factor of safety of slope stability from deformation energy," *Canadian Geotechnical Journal*, vol. 55, no. 1, pp. 296–302, 2018.

[22] F. Feng, X. B. Li, J. Rostami, D. X. Peng, D. Y. Li, and K. Du, "Numerical investigation of hard rock strength and fracturing under polyaxial compression based on Mogi-Coulomb failure criterion," *International Journal of Geomechanics*, vol. 19, no. 4, Article ID 04019005, 2019.

[23] J. M. Duncan and S. G. Wright, *Soil Strength and Slope Stability*, John Wiley & Sons, Hoboken, NJ, USA, 2nd edition, 2014.

[24] Y. Tu, X. Liu, Z. Zhong, and Y. Li, "New criteria for defining slope failure using the strength reduction method," *Engineering Geology*, vol. 212, pp. 63–71, 2016.

[25] O. C. Li and R. L. Taylor, *The finite element method*, Vol. 1, McGraw-Hill, New York, NY, USA, 4th edition, 1989.

[26] D. V. Griffiths and R. M. Marquez, "Three-dimensional slope stability analysis by elasto-plastic finite elements," *Géotechnique*, vol. 57, no. 6, pp. 537–546, 2007.

[27] D. V. Griffiths, J. Huang, and G. F. deWolfe, "Numerical and analytical observations on long and infinite slopes," *International Journal for Numerical and Analytical Methods in Geomechanics*, vol. 35, no. 5, pp. 569–585, 2011.

[28] D. W. Taylor, "Stability of earth slopes," *Boston Society of Civil Engineers*, vol. 24, no. 3, pp. 337–386, 1937.

[29] R. L. Michalowski, "Stability charts for uniform slopes," *Journal of Geotechnical and Geoenvironmental Engineering*, vol. 128, no. 4, pp. 351–355, 2002.

[30] R. L. Michalowski and T. Martel, "Stability charts for 3D failures of steep slopes subjected to seismic excitation," *Journal Geotechnical Geoenvironmental Engineering*, vol. 137, pp. 183–189, 2011.

[31] E. Stockton, B. A. Leshchinsky, M. J. Olsen, and T. M. Evans, "Influence of both anisotropic friction and cohesion on the formation of tension cracks and stability of slopes," *Engineering Geology*, vol. 249, pp. 31–44, 2019.

[32] S. Javankhoshdel and R. J. Bathurst, "Simplified probabilistic slope stability design charts for cohesive and cohesive-frictional (c-ϕ) soils," *Canadian Geotechnical Journal*, vol. 51, no. 9, pp. 1033–1045, 2014.

[33] S. Javankhoshdel and R. J. Bathurst, "Influence of cross correlation between soil parameters on probability of failure of simple cohesive and c-ϕ slopes," *Canadian Geotechnical Journal*, vol. 53, no. 5, pp. 839–853, 2016.

[34] Y. Zhang, G. Chen, L. Zheng, Y. Li, and X. Zhuang, "Effects of geometries on three-dimensional slope stability," *Canadian Geotechnical Journal*, vol. 50, no. 3, pp. 233–249, 2013.

[35] R. Baker, "A second look at taylor's stability chart," *Journal of Geotechnical and Geoenvironmental Engineering*, vol. 129, no. 12, pp. 1102–1108, 2003.

[36] A. J. Li, A. V. Lyamin, and R. S. Merifield, "Seismic rock slope stability charts based on limit analysis methods," *Computers and Geotechnics*, vol. 36, no. 1-2, pp. 135–148, 2009.

[37] Y. F. Gao, F. Zhang, and G. H. Lei, "An extended limit analysis of three-dimensional slope stability," *Géotechnique*, vol. 63, no. 6, pp. 518–524, 2013.

[38] H. T. Li, "Stability charts for uniform slopes in soils with nonlinear failure envelopes," *Engineering Geology*, vol. 168, pp. 38–45, 2014.

[39] R. Kalatehjari, A. Arefnia, A. S. Rashid, N. Ali, and M. Hajihassani, "Determination of three-dimensional shape of failure in soil slopes," *Canadian Geotechnical Journal*, vol. 52, no. 9, pp. 1283–1301, 2015.

[40] H. Zhu, D. V. Griffiths, G. A. Fenton, and L. M. Zhang, "Undrained failure mechanisms of slopes in random soil," *Engineering Geology*, vol. 191, pp. 31–35, 2015.

[41] Z. B. Sun, J. F. Li, Q. J. Pan, D. Dias, S. Q. Li, and C. Q. Hou, "Discrete kinematic mechanism for nonhomogeneous slopes and its application," *International Journal of Geomechanics*, vol. 18, no. 12, Article ID 04018171, 2018.

[42] C. C. Li and P. M. Jiang, "Failure mechanism of two-layered slopes subjected to the surcharge load," *International Journal of Geomechanics*, vol. 20, no. 2, Article ID 06019024, 2020.

[43] I. M. Smith, D. V. Griffiths, and L. Margetts, *Programming the Finite Element Method*, John Wiley & Sons, Chichester, UK, 2015.

[44] Y.-C. Li, Y.-M. Chen, T. L. T. Zhan, D.-S. Ling, and P. J. Cleall, "An efficient approach for locating the critical slip surface in slope stability analyses using a real-coded genetic algorithm," *Canadian Geotechnical Journal*, vol. 47, no. 7, pp. 806–820, 2010.